Check for updates

AGU ADVANCING EARTH AND SPACE SCIENCE

JGR Atmospheres

RESEARCH ARTICLE
10.1029/2022JD037581

**Special Section:**
The Exceptional Arctic Polar Vortex in 2019/2020: Causes and Consequences

# An Unprecedented Arctic Ozone Depletion Event During Spring 2020 and Its Impacts Across Europe

**Boyan H. Petkov[1,2], Vito Vitale[2], Piero Di Carlo[1,3], Oxana Drofa[4], Daniele Mastrangelo[4], Andrew R. D. Smedley[5], Henri Diémoz[6], Anna Maria Siani[7], Ilias Fountoulakis[8], Ann R. Webb[5], Alkiviadis Bais[9], Richard Kift[5], John Rimmer[5], Giuseppe Rocco Casale[7], Georg H. Hansen[10], Tove Svendby[10], Andrea Pazmiño[11], Rolf Werner[12], Atanas M. Atanassov[12], Kamil Láska[13], Hugo De Backer[14], Alexander Mangold[14], Ulf Köhler[15], Voltaire A. Velazco[15], René Stübi[16], Anna Solomatnikova[17], Kseniya Pavlova[17], Piotr S. Sobolewski[18], Bjørn Johnsen[19], Florence Goutail[11], Oliver Mišaga[20], Eleonora Aruffo[1,3], Ladislav Metelka[21], Zoltán Tóth[22], Dénes Fekete[23], Alexandr A. Aculinin[24], Angelo Lupi[2], Mauro Mazzola[2], and Federico Zardi[2]**

[1]Department of Advanced Technologies in Medicine & Dentistry, University G. d'Annunzio, Chieti-Pescara, Italy, [2]Institute of Polar Sciences, National Research Council, Bologna, Italy, [3]Center for Advanced Studies and Technology– CAST, Chieti, Italy, [4]National Research Council, Institute of Atmospheric Sciences and Climate (CNR-ISAC), Bologna, Italy, [5]Department of Earth and Environmental Sciences, University of Manchester, Manchester, UK, [6]ARPA Valle d'Aosta, Aosta, Italy, [7]Now at Independent researcher, Department of Physics, Sapienza University of Rome, Rome, Italy, [8]Institute for Astronomy, Astrophysics, Space Applications and Remote Sensing, National Observatory of Athens (IAASARS/NOA), Athens, Greece, [9]Laboratory of Atmospheric Physics, Aristotle University of Thessaloniki, School of Physics, Thessaloniki, Greece, [10]Norwegian Institute for Air Research (NILU), Atmosphere and Climate Department, Instituttveien 18, Kjeller, Norway, [11]LATMOS/CNRS–Université Versailles St Quentin, Guyancourt, France, [12]Space Research and Technology Institute, Bulgarian Academy of Sciences, Stara Zagora Department, Stara Zagora, Bulgaria, [13]Department of Geography, Faculty of Science, Masaryk University, Brno, Czech Republic, [14]Royal Meteorological Institute of Belgium, Brussels, Belgium, [15]Meteorological Observatory Hohenpeissenberg, Hohenpeissenberg, Germany, [16]Federal Office of Meteorology and Climatology, Payerne, Switzerland, [17]Voeikov Main Geophysical Observatory, Laboratory of Ozone Layer Control, St. Petersburg, Russia –GGO, [18]Department of Atmospheric Physics, Institute of Geophysics Polish Academy of Sciences, Warsaw, Poland, [19]Norwegian Radiation and Nuclear Safety Authority, Østerås, Norway, [20]Centre of Aerology and Solar Radiation, Slovak Hydrometeorological Institute, Poprad-Gánovce, Slovakia, [21]Solar and Ozone Observatory, Czech Hydrometeorological Institute Hvězdárna 456, Hradec Králové 8, Czech Republic, [22]H-ION Research, Development and Innovation Ltd., Budapest, Hungary, [23]Marczell György Main Observatory, Hungarian Meteorological Service, Budapest, Hungary, [24]Institute of Applied Physics (IAP), Chişinău, Moldova

**Key Points:**

- The 2020 ozone depletion in the Arctic was found to impact the ozone in the mid-latitude European areas
- The magnitude of ozone decrease in the southern regions declined with respect to that in the Arctic and occurred with a delay up to 20 days
- Such a response was similar to that observed in 2011 and both were considered a result of ozone-poor air masses transported southward

**Correspondence to:**
B. H. Petkov,
b.petkov@isac.cnr.it

**Citation:**
Petkov, B. H., Vitale, V., Di Carlo, P., Drofa, O., Mastrangelo, D., Smedley, A. R. D., et al. (2023). An unprecedented Arctic ozone depletion event during spring 2020 and its impacts across Europe. *Journal of Geophysical Research: Atmospheres*, *128*, e2022JD037581. https://doi.org/10.1029/2022JD037581

Received 2 AUG 2022
Accepted 13 JAN 2023

**Abstract** The response of the ozone column across Europe to the extreme 2020 Arctic ozone depletion was examined by analyzing ground-based observations at 38 European stations. The ozone decrease at the northernmost site, Ny-Ålesund (79°N) was about 43% with respect to a climatology of more than 30 years. The magnitude of the decrease declined by about 0.7% deg$^{-1}$ moving south to reach nearly 15% at 40°N. In addition, it was found that the variations of the ozone column at each of the selected stations in March-May were similar to those observed at Ny-Ålesund but with a delay increasing to about 20 days at mid-latitudes with a gradient of approximately 0.5 days deg$^{-1}$. The distributions of reconstructed ozone column anomalies over a sector covering a large European area show decreasing ozone that started from the north at the beginning of April 2020 and spread south. Such behavior was shown to be similar to that observed after the Arctic ozone depletion in 2011. Stratospheric dynamical patterns in March–May 2011 and during 2020 suggested that the migration of ozone-poor air masses from polar areas to the south after the vortex breakup caused the observed ozone responses. A brief survey of the ozone mass mixing ratios at three stratospheric levels showed the exceptional strength of the 2020 episode. Despite the stronger and longer-lasting Arctic ozone loss in 2020, the analysis in this work indicates a similar ozone response at latitudes below 50°N to both 2011 and 2020 phenomena.

**Plain Language Summary** The winter polar vortex isolates a huge volume of air from external impacts that, in the absence of the sunlight, leads to a great deal of cooling and the formation of polar stratospheric clouds. Chemical reactions taking place in these clouds contribute to ozone destruction. Such spring-time ozone depletions are regularly observed in Antarctica, but usually do not occur in the Arctic where the vortex is much less intense. However, in the past three decades several similar episodes occurred in the Arctic and the most marked of them took place in the 2011 and 2020 springs. The response of the ozone

© 2023. The Authors.
This is an open access article under the terms of the Creative Commons Attribution License, which permits use, distribution and reproduction in any medium, provided the original work is properly cited.

21698996, 2023, 3, Downloaded from https://agupubs.onlinelibrary.wiley.com/doi/10.1029/2022JD037581 by CochraneItalia, Wiley Online Library on [31/01/2023]. See the Terms and Conditions (https://onlinelibrary.wiley.com/terms-and-conditions) on Wiley Online Library for rules of use; OA articles are governed by the applicable Creative Commons License

21698996, 2023, 3, Downloaded from https://agupubs.onlinelibrary.wiley.com/doi/10.1029/2022JD037581 by CochraneItalia, Wiley Online Library on [31/01/2023]. See the Terms and Conditions (https://onlinelibrary.wiley.com/terms-and-conditions) on Wiley Online Library for rules of use; OA articles are governed by the applicable Creative Commons License

layer over Europe to the 2020 episode was studied here by analyzing the data from 38 ground measurement stations. It was found that there was a nearly 43% decrease in ozone in the Arctic, and, as it spread southward, a reduction of 15% in mid-latitudes 15–20 days later. This spread was attributed to the transport of ozone-poor air from the Arctic to the south after the vortex breakup. Despite the stronger depletion in 2020 and some differences in the movement of air, the response of the ozone layer was quite similar in the springs of both 2011 and 2020.

## 1. Introduction

The monitoring of ozone depletion episodes in the Antarctic that started in the early 1980s has shown their frequency of occurrence and intensity to be relatively stable (Farman et al., 1985; Solomon et al., 2014; WMO, 2018). These phenomena take place during the late austral winter and early spring over an area that covers practically the entire Antarctic continent. A depletion episode is initiated when a vortex forms isolating the polar stratosphere from the lower latitude air masses and, in the absence of solar radiation, causes a decrease in temperature. When the temperature gets below the chlorine activation threshold, $T_{act}$ (approximately 196 K) and causes the formation of polar stratospheric clouds (PSCs), the chemical destruction of ozone in the lower stratosphere intensifies (Crutzen & Arnold, 1986; Harris et al., 2010; Molina & Rowland, 1974; Solomon et al., 2014; Tilmes et al., 2006; WMO, 2010; WMO, 2018). In contrast to the Antarctic, the Arctic polar vortex is usually unstable due to dynamic phenomena, like Rossby waves (Hauchecorne et al., 2002; WMO, 2007). As a result, pronounced ozone depletion events in the Arctic have occurred only occasionally and their strengths varied appreciably during winter and spring (Solomon et al., 2007). However, several episodes similar to those observed in the Antarctic have taken place in the past few decades, when unusually stable polar vortices were observed in the springs of 1993, 1996, 1997, 2000, 2005, 2011, and 2020 (Arnone et al., 2012; Hauchecorne et al., 2002; Koch et al., 2004; Manney et al., 1994; Rösevall et al., 2008; WMO, 2007). Of these, the last two episodes together with that in 1997 were found to be extremely strong (Coy et al., 1997; Manney et al., 2011, 2020; Lawrence et al., 2020) as illustrated in Figure 8.

In contrast to preceding events, the 2011 Arctic vortex caused an atypically long cold period in the stratosphere that lasted until the end of March. Temperatures in the lower stratosphere stayed below $T_{act}$ for more than 100 days (Manney et al., 2011). Similar to the 2011 episode, the strong polar vortex in spring 2020 also created conditions favorable for ozone depletion. While in 2011 the maximum ozone loss occurred at 480–500 K potential temperature levels (about 19–20 km height) in 2020 ozone loss took place at 440–460 K (approximately 17–18 km). In this case, higher atmospheric pressure contributed to a stronger effect on the ozone column content which was one of the main causes leading to higher depletion in 2020 (Manney et al., 2020).

Compared to Antarctica where chemistry is considered the leading factor for ozone depletion, such a phenomenon in the Arctic is due to both chemistry and dynamics (Von der Gathen et al., 2021). Some authors (Strahan et al., 2013, 2016; Tegtmeier et al., 2008) argued almost equal weight of these two factors, while Isaksen et al. (2012) reported only a 23% contribution of chemical ozone loss in the 2011 event, with the primary cause of the observed low ozone being considered the weakened transport from mid-latitudes due to the anomalously strong polar vortex. Owing to the enhanced role of dynamical processes on the ozone abundance in the Arctic stratosphere, Chipperfield and Jones (1999) assumed that future circulation changes could make the Arctic vortex more Antarctic-like which would significantly affect the mean winter ozone. Taken together, these results suggest that atmospheric dynamics would impact the ozone distribution over large areas in the northern hemisphere after the vortex breakup.

The effect of the Arctic ozone depletion events on lower-latitude ozone has been studied by both model assessments and analyses of the results from field measurements (Hauchecorne et al., 2002; Knudsen & Grooß, 2000; Koch et al., 2004; Whaley et al., 2013). Petkov et al. (2014) examined the response of the ozone column over Europe to the 2011 event by analyzing a set of ground-based observations and found a 15%–18% decrease in the ozone column compared to the mid-latitude climatology that was attributable to Arctic processes. The mid-latitude ozone minima occurred with a delay of about 2 weeks compared to that in the Arctic and the ozone decrease was viewed as a result of air mass transport in the lower stratosphere taking place after the vortex breakup. Signs of similar mid-latitude ozone response to the 2020 event was also observed in the ozone column evolution registered at six European stations distributed from the Arctic to middle latitudes (Petkov et al., 2021). The present work

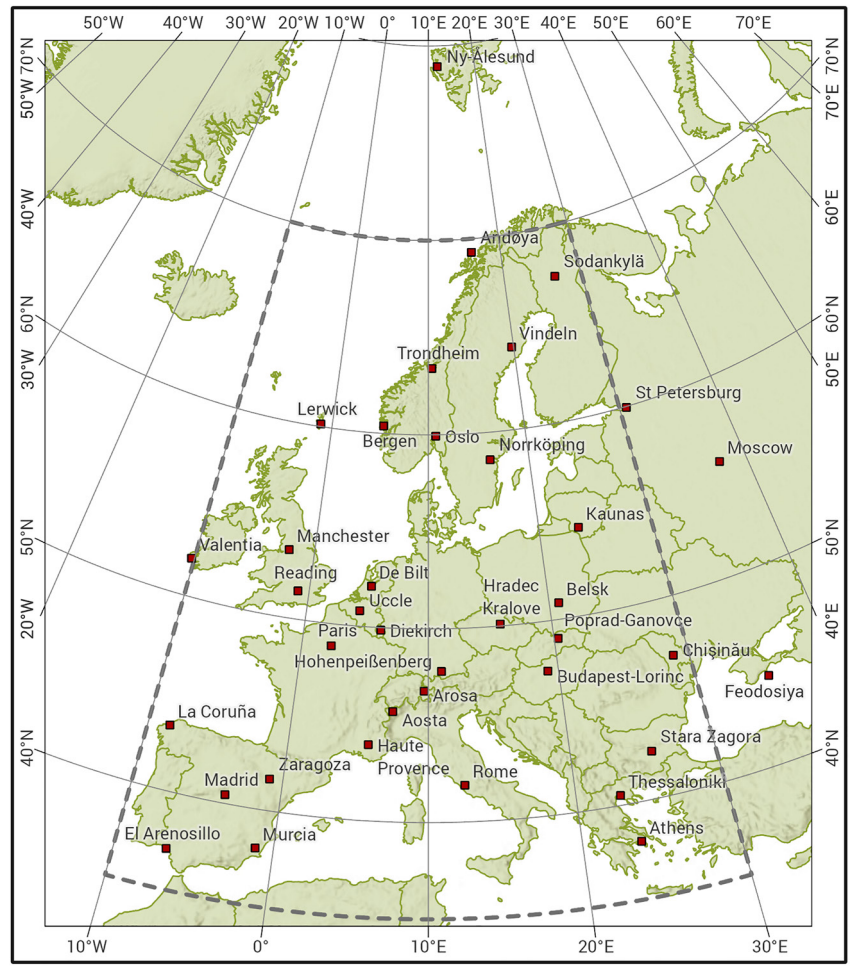


**Figure 1.** The geographical position of the stations considered in the present study. The dashed curves outline the sector over which the ozone column distribution was reconstructed (see Figure 6).

aims to perform a more detailed analysis of the ozone response to the 2020 depletion by applying the approach used for studying the 2011 episode. The results of such an analysis are presented and discussed in Section 3, while Section 4 compares the 2011 and 2020 episodes in light of air mass transport after the vortices broke down.

## 2. Data Sets

The effects of Arctic ozone depletion across Europe were examined by using ozone column observations at 38 European stations as mapped in Figure 1 and listed in Table 1. Data for 35 of the stations were taken from the World Ozone and Ultraviolet Data Center (WOUDC, 2020), while the measurements at Trondheim, Bergen and part of the results from Ny-Ålesund were provided by the Norwegian UV monitoring network that uses GUV-541 radiometers (Svendby et al., 2021). Data from the narrow-band filter radiometer UV-RAD (Petkov et al., 2006) operating at Ny-Ålesund, were provided by the Institute of Polar Sciences at the Italian National Research Council (CNR-ISP). The observations made by GUV 2511 located at Stara Zagora that were used only for the reconstruction of ozone anomalies distribution in the spring 2020 (Figure 6) were provided by the Space Research and Technology Institute at the Bulgarian Academy of Sciences.

The majority of instruments in the WOUDC database are Brewer and Dobson spectrophotometers (see Table 1) while some of the stations are equipped with SAOZ spectrometers (Pommereau & Goutail, 1988), filter ozonometers M-124 (Nerobelov et al., 2022), and Microtops II (Morys et al., 2001). All above listed instruments are well characterized and periodically calibrated against reference devices to provide reliable data. The review of the WOUDC data set made by Koukouli et al. (2015) reported a systematic difference of 0.6% between Brewer and



21698996, 2023, 3, Downloaded from https://agupubs.onlinelibrary.wiley.com/doi/10.1029/2022JD037581 by Cochraneltalia, Wiley Online Library on [31/01/2023]. See the Terms and Conditions (https://onlinelibrary.wiley.com/terms-and-conditions) on Wiley Online Library for rules of use; OA articles are governed by the applicable Creative Commons License

21698996, 2023, 3, Downloaded from https://agupubs.onlinelibrary.wiley.com/doi/10.1029/2022JD037581 by CochraneItalia, Wiley Online Library on [31/01/2023]. See the Terms and Conditions (https://onlinelibrary.wiley.com/terms-and-conditions) on Wiley Online Library for rules of use; OA articles are governed by the applicable Creative Commons License

**Table 1**
*The Stations That Were Taken Into Account in the Present Study, Given With Their Geographical Coordinates and Indication of the Corresponding Instruments and Observational Periods*

| N | Station, country | Latitude, longitude | Instrument | Observational period $\Delta T_S$ |
|---|---|---|---|---|
| 1 | Ny-Ålesund, Norway | 78°55′ N, 11°55′ E | Dobson Beck 008 | 1966–1968 |
| | | | | 1995–1997 |
| | | | Brewer MKIV 050 | 2007–2009 |
| | | | | 2013–2020 |
| | | | GUV-541 | 1995–2020 |
| | | | SAOZ | 1991–2020 |
| | | | UV-RAD | 2008–2020 |
| 2 | Andøya, Norway | 69°18′N, 16°00′E | Brewer MKIII 104 | 2000–2020 |
| 3 | Sodankylä, Finland | 67°22′ N, 26°37′ E | SAOZ | 1990–2020 |
| | | | Brewer MKII 037 | 1988–2010 |
| 4 | Vindeln, Sweden | 64°14′ N, 19°46′ E | Brewer MKII 006 | 1996–2020 |
| | | | Dobson Beck 030 | 1991–2020 |
| 5 | Trondheim, Norway | 63°25′ N, 10°24′ E | GUV-541 | 1996–2020 |
| 6 | Bergen, Norway | 60°23′ N, 5°20′ E | GUV-541 | 1996–2020 |
| 7 | Lerwick, UK | 60°08′ N, 01°11′ W | Dobson Beck 007 | 1952–1966 |
| | | | Dobson Beck 032 | 1968–2014 |
| | | | | 2016–2020 |
| | | | Dobson Beck 035 | 1994–1998 |
| | | | Dobson Beck 041 | 2007–2014 |
| | | | | 2016–2017 |
| 8 | Saint Petersburg, Russia | 59°57′ N, 30°42′ E | Filter M-83 | 1973–1984 |
| | | | Filter M-124 | 1985–2015 |
| | | | | 2017–2020 |
| 9 | Oslo, Norway | 59°56′ N, 10°43′ E | Brewer MKV 042 | 1990–2020 |
| | | | Dobson Beck 056 | 1969–1998 |
| 10 | Norrköping, Sweden | 58°35′ N, 16°09′ E | Brewer MKIII 128 | 1996–2020 |
| | | | Brewer MKII 006 | 1988–1996 |
| 11 | Moscow, Russia | 55°45′ N, 37°34′ E | Dobson Beck 107 | 1991–2004 |
| | | | Filter M-124 | 1984–2004 |
| | | | | 2014–2020 |
| | | | Filter M-83 | 1973–1984 |
| | Obninsk, Russia | 55°07′ N, 36°18′ E | Brewer MKII 044 | 1996–2001 |
| | | | | 2004–2007 |
| | | | | 2009–2016 |
| 12 | Kaunas, Lithuania | 54°31′ N, 23°32′ E | Brewer MKIII 219 | 2018–2020 |
| | | | Filter M-124 | 1993–2018 |
| 13 | Manchester, UK | 53°29′ N, 02°14′ W | Brewer MKIII 172 | 2000–2020 |
| 14 | De Bilt, Netherlands | 52°06′ N, 05°11′ E | Brewer MKIII 100 | 1994–2006 |
| | | | Brewer MKIII 189 | 2006–2020 |
| 15 | Belsk, Poland | 51°50′ N, 20°47′ E | Brewer MKII 064 | 1994–2005 |
| | | | Dobson 084 | 1963–2020 |

**Table 1**
*Continued*

| N | Station, country | Latitude, longitude | Instrument | Observational period $\Delta T_S$ |
|---|---|---|---|---|
| 16 | Valentia, Ireland | 51°56′ N, 10°15′ W | Brewer MKIII 227 | 2016–2020 |
| | | | Brewer MKIV 088 | 1993–2020 |
| 17 | Reading, UK | 51°27′ N, 00°56′ W | Brewer MKIV 075 | 2002–2020 |
| | | | Brewer MKII 126 | 2010–2011 |
| 18 | Uccle, Belgium | 50°48′ N, 04°21′ E | Brewer MK III 178 | 2001–2020 |
| | | | Brewer MK III 100 | 2010, 2020 |
| | | | Brewer MK II 016 | 1983–2020 |
| | | | Dobson 040 | 1952–2009 |
| 19 | Hradec Kralove, Czech Republic | 50°06′ N, 15°50′ E | Brewer MK III 199 | 2020 |
| | | | Brewer MK III 184 | 2004–2020 |
| | | | Brewer MK IV 098 | 1994–2020 |
| | | | Dobson 084 | 1961–2020 |
| 20 | Diekirch, Luxembourg | 49°52′ N, 06°10′ E | Microtops II 5375 | 2003–2020 |
| | | | Microtops II 1383, 3,012 | 2001–2003 |
| 21 | Poprad-Ganovce, Slovakia | 49°02′ N, 20°19′ E | Brewer MK IV 097 | 1993–2020 |
| 22 | Paris, France | 48°50′ N, 02°21′ E | SAOZ | 2005–2020 |
| 23 | Hohenpeißenberg, Germany | 47°48′ N, 11°01′ E | Brewer MK II 010 | 1984–2020 |
| | | | Dobson 104 | 1967–2020 |
| 24 | Budapest-Lorinc, Hungary | 47°26′ N, 19°11′ E | Brewer MKII 152 | 1999–2020 |
| | | | Dobson 110 | 1970–1998 |
| | | | M-83 | 1967–1969 |
| 25 | Chişinău, Moldova | 47°00′ N, 28°49′ E | Microtops II 7351 | 2003–2020 |
| 26 | Arosa, Switzerland (these instruments have been operating in Davos after 2013) | 46°47′ N, 09°41′ E | Dobson Beck 002 | 1926–1929 |
| | | | | 1932–1949 |
| | | | Dobson Beck 015 | 1949–1986 |
| | | | Dobson Beck 101 | 1986–2013 |
| | | | Brewer MKII 040 | 1988–2013 |
| | Davos, Switzerland | 46°48′ N, 09°50′ E | Brewer MKIII 163 | 2014–2020 |
| 27 | Aosta, Italy | 45°42′ N, 07°22′ E | Brewer MKIV 066 | 2007–2020 |
| 28 | Feodosiya, Ukraine | 44°32′ N, 35°07′ E | Filter M-83 | 1973–1980 |
| | | | Filter M-124 | 1984–1995 |
| | | | | 1998 |
| | | | | 2019–2020 |
| 29 | Haute Provence, France | 43°56′ N, 05°42′ E | Dobson 085 | 1983–2018 |
| | | | SAOZ | 1992–2020 |
| 30 | La Coruña, Spain | 43°20′ N, 08°28′ W | Brewer MKIV 151 | 1999–2014 |
| | | | Brewer MKIV 070 | 2009–2014 |
| | | | | 2017–2020 |
| 31 | Stara Zagora, Bulgaria[a] | 42°26′N, 25°38′E | GUV 2511 | 2015–2020 |
| 32 | Rome University, Italy | 41°54′ N, 12°31′ E | Brewer MKIV 067 | 1992–2020 |
| 33 | Zaragoza, Spain | 41°38′ N, 00°55′ W | Brewer MKIV 166 | 2000–2020 |
| 34 | Thessaloniki, Greece | 40°31′ N, 22°58′ E | Brewer MKII 005 | 1982–2020 |



21698996, 2023, 3, Downloaded from https://agupubs.onlinelibrary.wiley.com/doi/10.1029/2022JD037581 by CochraneItalia, Wiley Online Library on [31/01/2023]. See the Terms and Conditions (https://onlinelibrary.wiley.com/terms-and-conditions) on Wiley Online Library for rules of use; OA articles are governed by the applicable Creative Commons License

21698996, 2023, 3, Downloaded from https://agupubs.onlinelibrary.wiley.com/doi/10.1029/2022JD037581 by CochraneItalia, Wiley Online Library on [31/01/2023]. See the Terms and Conditions (https://onlinelibrary.wiley.com/terms-and-conditions) on Wiley Online Library for rules of use; OA articles are governed by the applicable Creative Commons License

**Table 1**
*Continued*

| N | Station, country | Latitude, longitude | Instrument | Observational period $\Delta T_S$ |
|---|---|---|---|---|
| 35 | Madrid, Spain | 40°27′ N, 03°43′ W | Brewer MKIV 070 | 1991–2016 |
| | | | Brewer MKIV 186 | 2008–2020 |
| 36 | Murcia, Spain | 38°00′ N, 01°10′ W | Brewer MKIV 117 | 1995–2020 |
| 37 | Athens, Greece | 37°59′ N, 23°47′ E | Brewer MKIV 001 | 2003–2020 |
| 38 | El Arenosillo, Spain | 37°06′ N, 06°44′ W | Dobson Beck 120 | 1976–2014 |
| | | | Brewer MKIII 150 | 2000–2020 |

[a]The data were used only to reconstruct of the ozone distribution in 2020 (Figure 6).

Dobson instruments that can increase to 2% in winter months. A comparison among Brewer and Dobson records at the stations in Table 1 equipped with both devices showed a bias of 1%. A similar comparison between Dobson and SAOZ, carried out at Haute Provence gives a discrepancy of 1%, while at Sodankylä and Ny-Ålesund the difference between Brewer and SAOZ was found to be 3% and 1% respectively. In the framework of an intercomparison campaign GUV and UV-RAD operating at Ny-Ålesund showed discrepancies of no more than 3% with respect to Brewer (Petkov et al., 2019). The harmonized data set of the Norwegian GUV network showed a bias of 0.3% with respect to Brewers that could vary up to 2% (Svendby et al., 2021). The filter ozonometer M-124 used in Saint Petersburg showed no bias with respect to Dobson measurements (Nerobelov et al., 2022) while a similar comparison made at Moscow (Table 1) indicates a discrepancy of 2%.

Time series at the selected stations are a result of long-term, routine observations with relatively few breaks. A significant gap of data was found at Moscow, where measurements between 2004 and 2013 are absent. This time interval can be covered by the data from Obnisk that is about 100 km from Moscow; at such distances corresponding ozone columns are highly correlated (Bojkov & Fioletov, 1995). In fact, the bias of the data provided by the Brewer at Obnisk and the Dobson at Moscow for the period of their simultaneous working was estimated to be 1% while the discrepancy between the same Brewer and M-124 at Moscow was 3%. These deviations are very close to the usual biases among the instruments that allows us to unite the data of both the stations. A similar interruption of the measurements occurred at Arosa, where the observations after 2013 were relocated to Davos. However, in this case the distance between two sites is only about 10 km (Gröbner et al., 2021).

To investigate the evolution of the ozone and dynamic processes in the stratosphere during the springs of 2011 and 2020, geopotential height, daily ozone column, and monthly mean ozone mass mixing ratios at 100 hPa, 50 hPa, and 30 hPa were considered. These data were provided by the ERA-5 reanalyses performed by the European Center for Medium-Range Weather Forecasts (ECMWF, 2021) for the period from 1979 to 2020.

The goals of the present work were pursued through statistical analysis of the above data sets by introducing appropriate parameters and the results are presented in the following sections.

## 3. Response of the Ozone Column Over Europe to the 2020 Arctic Depletion

The behavior of the ozone column in Europe in spring 2020 was studied by analyzing the long-term records obtained from the stations in Figure 1 and Table 1. The reduction in the ozone amount associated with the Arctic depletion was characterized by the relative ozone loss and its duration, both determined at each of the stations. In addition, the distributions of daily ozone anomalies with respect to the corresponding climatological levels over the sector indicated in Figure 1 were reconstructed for April and May in order to give an overview of the European ozone response to the 2020 Arctic event.

### 3.1. Characteristics of the Ozone Column Variations at the Selected Stations

Similar to the approach followed by Petkov et al. (2014), the relative ozone column variations $R_{S,Y}(t_D)$ at the station $S$ placed at latitude $\varphi$ and longitude $\lambda$ for a day $t_D$ of year $Y$ were calculated as

$$R_{S,Y}(t_D) = \frac{Q_{S,Y}(t_D)}{Q_S(t_D)}, \quad (1)$$

21698996, 2023, 3, Downloaded from https://agupubs.onlinelibrary.wiley.com/doi/10.1029/2022JD037581 by CochraneItalia, Wiley Online Library on [31/01/2023]. See the Terms and Conditions (https://onlinelibrary.wiley.com/terms-and-conditions) on Wiley Online Library for rules of use; OA articles are governed by the applicable Creative Commons License

where $Q_{S,Y}(t_D)$ is the daily mean ozone column. The denominator $Q_S(t_D)$ represents the median $Q_{S,Y}(t_D)$ found at station $S$ for the same day $t_D$ of all the years $Y$ pertaining to the observational period $\Delta T_S$ given in Table 1. The assessment of $Q_S(t_D)$ used all data from a station $S$, excluding only the years found to have relatively strong Arctic ozone depletions (1997, 2011 and 2020, see Section 1). The ratio $R_{S,Y}(t_D)$ expresses the ozone column changes at a certain location with respect to the average ozone level at the same location. In the large latitudinal range considered in the present analysis these average levels are usually different for different latitudes as Figure 8 illustrates for 1979 and 2019 which present the usual ozone behavior. Thus, the ratios $R_{S,Y}(t_D)$ were considered to secure a more realistic comparison among the ozone variations registered at the stations given in Figure 1. The biases among the different instruments operating at some of the stations, reported in Section 2 were assumed to be of minor importance in the present analysis.

Figure 2 presents time patterns of $R_{S,Y}(t_D)$ evaluated for several stations at different latitudes. To better illustrate the behavior of the 2020 ozone evolution, the 95% confidence interval of $R_{S,Y}(t_D)$ obtained for all the years $Y \in \Delta T_S$ at each of the stations is indicated by the corresponding 2.5th and 97.5th percentile curves, smoothed by a running average procedure. As can be seen in Table 1 the time series at different stations have different lengths with predominant durations of 20–25 years. It is expected that such a difference in the time series lengths could impact the behavior of ratio $R_{S,Y}(t_D)$. To examine this possibility, the median $Q_S(t_D)$ was calculated for the period 2000–2019 at several stations characterized by significantly long records and the ratio found for this median was compared with the corresponding ratio $R_{S,Y}(t_D)$ found for the whole period $\Delta T_S$. These evaluations were performed for Arosa/Davos, Belsk, Hohenpeissenberg, Uccle and Hradec Kralove and the results are shown in Figure 2. It can be concluded that $Q_S(t_D)$ evaluated for the past 20-year period also provides a realistic assessment of the $R_{S,Y}(t_D)$ behavior.

In Figure 2a the left and right columns represent stations that depict two different paths both starting from the polar region and following the western and eastern bounds of the selected area to finish at mid-latitudes. Figure 2b further illustrates the ozone evolution at additional sites at latitudes between 42°N and 60°N. As can be seen from Figure 2a, the ozone column dropped by about 45% at the northernmost station Ny-Ålesund in 2020. Ozone started to decrease from the middle of March and the minimum occurred at the beginning of April maintaining this low level for the next 2 weeks. A rapid recovery started in the middle of the month and after slight oscillations the ozone returned to within its climatological range in early May although ozone remained close to the 2.5th percentile until July with sporadic minima below this bound. The period $\Delta t_{NyA}$ between the approximate initial date of the ozone decrease episode at Ny-Ålesund, 15 March, and the day when the ozone returned to the normal values, 5 May, is indicated by vertical dashed lines; both lines are extrapolated to all the stations presented in Figure 2. The figure shows the appearance of $R_{S,2020}(t_D)$ minima during the period of extreme Ny-Ålesund ozone reduction occurring at lower latitude stations. Such minima are lower than or very close to the 2.5th percentiles of the corresponding stations and the deepest decrease in the ozone column observed at a station $S$ can be evaluated in percent as:

$$Q_{\min}(S) = \min_{t_D}\left[(1 - R_{S,Y}(t_D)) \times 100\right] \tag{2}$$

with $t_D \in \Delta t_{NyA}$. In reality, the ozone column can be a subject of sharp day-to-day variations that would lead to unrealistic assessment of $Q_{\min}(S)$ and to avoid such an effect the $R_{S,Y}(t_D)$ curves were smoothed through a running average approach applied with a 5-day window before evaluations according to Equation 2. Figure 3 exhibits the patterns of $Q_{\min}(S)$ as a function of the station latitude $\varphi$ using data from all stations. Since the distance between the northernmost station and the other ones below 70°N is appreciably large (see Figure 1), a lack of observational points can be noted in this area. To fill this gap, $R_{S,Y}(t_D)$ curves were constructed using ERA-5 data sets for the 2000–2020 period and minima $Q_{\min}(S)$ were calculated for several points located on the same meridian as Ny-Ålesund station (12°E) and distributed from 77°N to 65°N as Figure 3 shows. It worth noting the good fitting of this points among those obtained from the ground observations. In addition, the best fit lines of the $Q_{\min}(\varphi)$ values is also presented in Figure 3 to outline the tendency of the minima. It can be seen that the depth of the ozone minima gradually decreased from about 43% in the Arctic to nearly 15% at 40°N. Such a decrease in ozone column causes a corresponding increase in the surface solar ultraviolet irradiance. For instance, it was found that the 2020 ozone depletion resulted in about 75% enhancement of the erythemal radiation in the Arctic in March and contributed to approximately 18% increase at Aosta (46°N), Italy in May (Bernhard et al., 2020; Petkov et al., 2021).

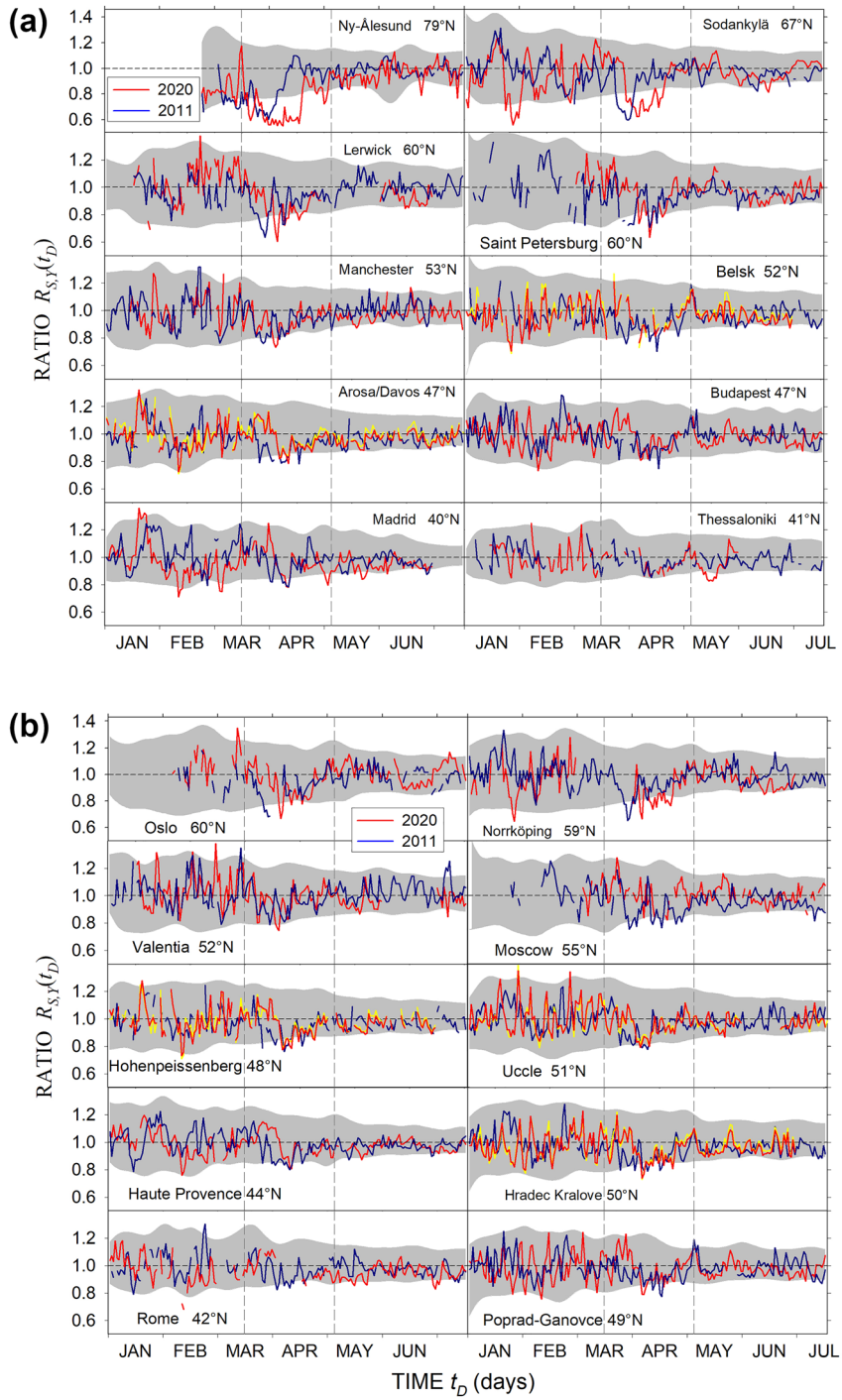


**Figure 2.** (a) Examples of the ratios $R_{S,2020}(t_D)$ and $R_{S,2011}(t_D)$ calculated for some of the selected stations, which are placed on two different north-south paths in Europe represented by the left and right columns, respectively (see Figure 1). (b) Additional examples of the ratios $R_{S,2020}(t_D)$ and $R_{S,2011}(t_D)$ calculated for several other stations in the central Europe. The yellow curves in the Arosa/Davos and Belsk panels in (a), and in the Hohenpeissenberg, Uccle and Hradec Kralove panels in (b) show the ratio $R_{S,2020}(t_D)$ assessed by using climatological evolution $Q_S(t_D)$ in Equation 1 calculated over the period from 2000 to 2019. The gray zones show the 95% confidence intervals of $R_{S,Y}(t_D)$ with $Y \in \Delta T_S$ bounded by the smoothed curves of the 2.5th and 97.5th percentiles, and the horizontal dashed lines indicate $R_{S,Y}(t_D) = 1$. The vertical dashed lines show the period of ozone decrease episode $\Delta t_{NyA}$ at Ny-Ålesund, in 2020 (from 15 March to 5 May), and extrapolated to all other stations.



21698996, 2023, 3, Downloaded from https://agupubs.onlinelibrary.wiley.com/doi/10.1029/2022JD037581 by CochraneItalia, Wiley Online Library on [31/01/2023]. See the Terms and Conditions (https://onlinelibrary.wiley.com/terms-and-conditions) on Wiley Online Library for rules of use; OA articles are governed by the applicable Creative Commons License

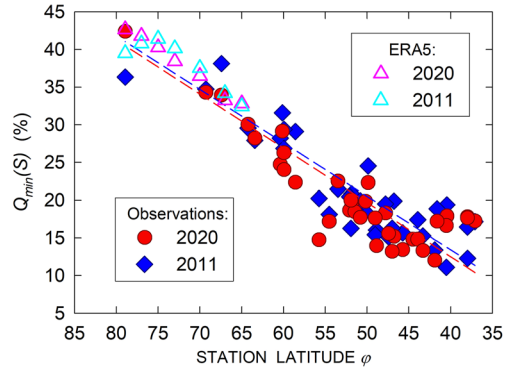


**Figure 3.** Percentage of the decrease in ozone column $Q_{\min}(S)$ estimated through Equation 2 that occurred at each of the considered stations $S$ located at latitude $\varphi$ in 2020 (red circles) during the period $\Delta t_{NyA}$ (see Figure 2). Analogous minima found for 2011 (blue circles) are also given for comparison. Open triangles show $Q_{\min}(\varphi)$ found from ERA-5 data set by following the same approach for 2020 (pink) and 2011 (cyan). Dashed lines represent linear best fits for 2020 (red) and 2011 (blue) with correlation coefficients 0.93 and 0.94, respectively. The corresponding equations are $(0.72 \pm 0.04)\varphi - 16.3$ and $(0.71 \pm 0.04)\varphi - 15.0$; the slope coefficients are given with their standard deviations.

Figure 2 shows that the ozone column reached a minimum at all stations by the beginning of April 2020 and after that returned to the corresponding climatological levels, a behavior that is quite similar to that observed at Ny-Ålesund. The next subsection discusses such a behavior of the ozone column observed at the sites selected in Table 1 during the spring of 2020.

### 3.2. Occurrence of the 2020 Ozone Column Decrease at Different Latitudes

A timeshift of the decreasing ozone phase can be seen moving south from the northernmost site in Figure 2. In fact, while the decrease of ozone at Ny-Ålesund occurred in the second half of March, a similar decrease started at the beginning of April in Madrid and Hradec Kralove, for instance. To study such a delay of the ozone decline episodes in southern Europe, the cross-correlation function (CCF) between time patterns of the relative ozone variations $R_{NyA,2020}(t_D)$ at Ny-Ålesund and $R_{S,2020}(t_D)$ at each of the other stations was evaluated for the period March-May 2020. This is shown in Figure 4, where four sites separated by about 10° latitude from each other were selected for illustration and the time series presenting $R_{NyA,2020}(t_D)$ and $R_{S,2020}(t_D)$ are shown in the left column. The corresponding CCFs are given on the right in Figure 4 and the lags $\Delta t_D$ of their maxima determine the delays $\tau_D(S)$ of the ozone reduction episode at station $S$ relative to that at Ny-Ålesund. The $\tau_D$-shifted curves, $R_{S,2020}(t_D - \tau_D(S))$, at the stations presented in the left column of Figure 4, and $R_{NyA,2020}(t_D)$ are noticeably

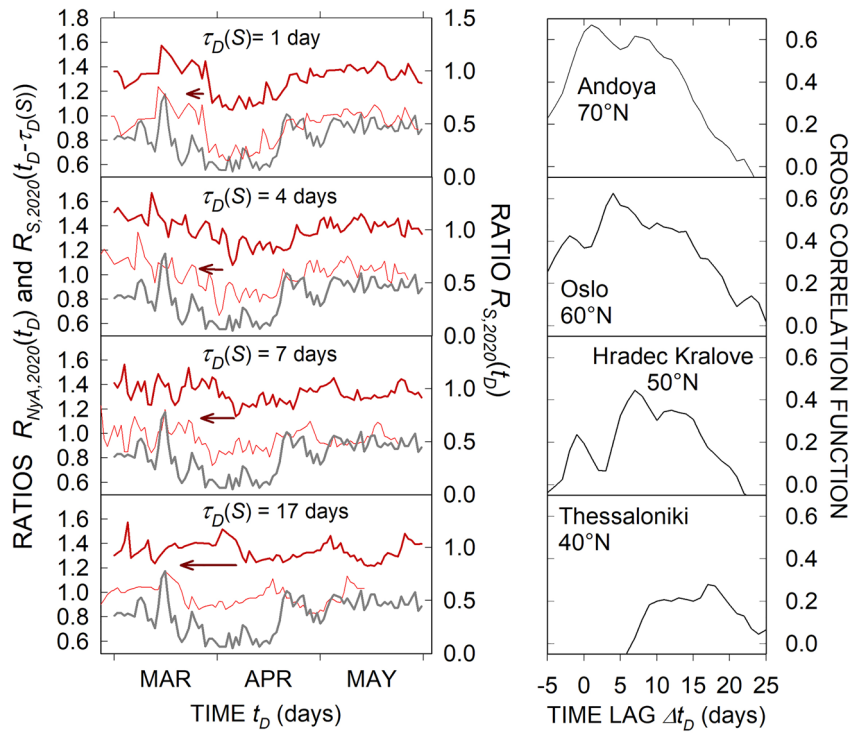


**Figure 4.** The panels in the left column compare the March-May behavior of the ratio $R_{NyA,2020}(t_D)$ (gray curves) calculated for Ny-Ålesund with the ratios $R_{S,2020}(t_D)$ (thick dark red curves) for the station $S$, scaled by the corresponding right ordinate axes. The right column exhibits CCFs between each of the pairs $R_{NyA,2020}(t_D)$ and $R_{S,2020}(t_D)$ that determine the corresponding delays $\tau_D(S)$ (the time lag $\Delta t_D$ of the CCF maximum), which are given in the left panels at the same rows. The ratios $R_{S,2020}(t_D - \tau_D(S))$ shown by the thin red curves are the ratios $R_{S,2020}(t_D)$ shifted to the left by $\tau_D(S)$ as schematically indicated by the arrows. The names and latitudes of the selected stations are given in the right column.



21698996, 2023, 3, Downloaded from https://agupubs.onlinelibrary.wiley.com/doi/10.1029/2022JD037581 by CochraneItalia, Wiley Online Library on [31/01/2023]. See the Terms and Conditions (https://onlinelibrary.wiley.com/terms-and-conditions) on Wiley Online Library for rules of use; OA articles are governed by the applicable Creative Commons License

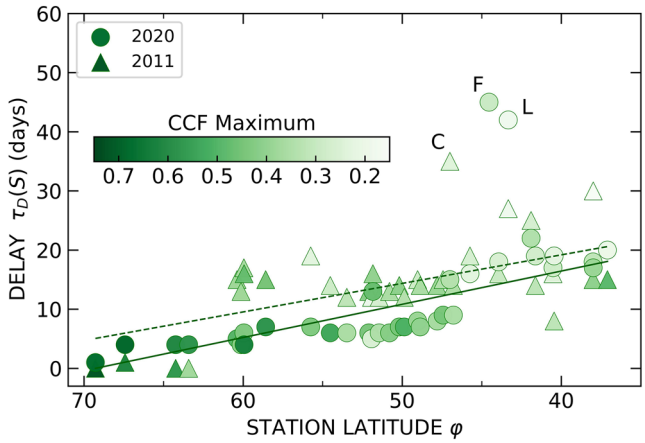


**Figure 5.** Delays $\tau_D(S)$ of the ozone column time patterns observed at each station in spring 2020 relative to Ny-Ålesund, as a function of the station latitudes $\varphi$. The value of the CCF maximum is represented in colors determined by the scale in the graph. Analogous delays calculated for 2011 are also presented for comparison. The $\tau_D(S)$ for La Coruña (L) and Feodosiya (F) in 2020, and for Chişinău (C) in 2011 that were found to largely deviate from the common trend are also indicated. Linear best fit approximations are presented by solid for 2020 and dashed for 2011 lines. The corresponding equations are $-(0.59 \pm 0.06)\varphi + 40.2$ and $-(0.48 \pm 0.01)\varphi + 38.5$ with correlation coefficients 0.86 and 0.63; the slope coefficients are given with their standard deviations and the above points L, F and C were excluded from the estimations.

similar. In other words, the ozone reduction episode at each station is representative of the reduction episode that occurred in the Arctic, but with a time delay and reduced amplitude.

The right column in Figure 4 shows a gradual displacement of the CCF maxima to larger lags for low-latitude sites, that is, an increase in the delays $\tau_D(S)$. At the same time, the maxima of CCFs decrease when moving south; this can be attributed to changes in the shape of $R_{S,2020}(t_D)$ curves due to increase in the ozone column minima as Figure 3 shows. On the other hand, the features of regional atmospheric dynamics modulate additional short-term variations that also contribute to the decrease in the CCFs maxima. However, the decreasing and recovering phases of the episode within the period $\Delta t_{NyA}$ observed at Ny-Ålesund can be recognized also in the southern stations with the corresponding delays $\tau_D(S)$. These delays together with the maxima of CCFs were estimated for each of the stations and are given as a function of the corresponding station latitude $\varphi$ in Figure 5. It is seen that the ozone over the 60°N–70°N region responded to the Arctic depletion with a delay of no more than 5 days, while the equivalent delay was from 5 to 15 days for the area between 45°N and 60°N. A delay ranging between 17 and 23 days was estimated for the stations below 45°N. An unusually high delay $\tau_D(S)$ was determined for Feodosiya and La Coruña as Figure 5 shows. A similar large value characterized the analogous delay $\tau_D(S)$ at Chişinău in 2011. These anomalous deviations can be accounted for by regional features of troposphere-stratosphere coupling that could affect the ozone evolution especially since the stations are placed in contrasting areas; two of them are

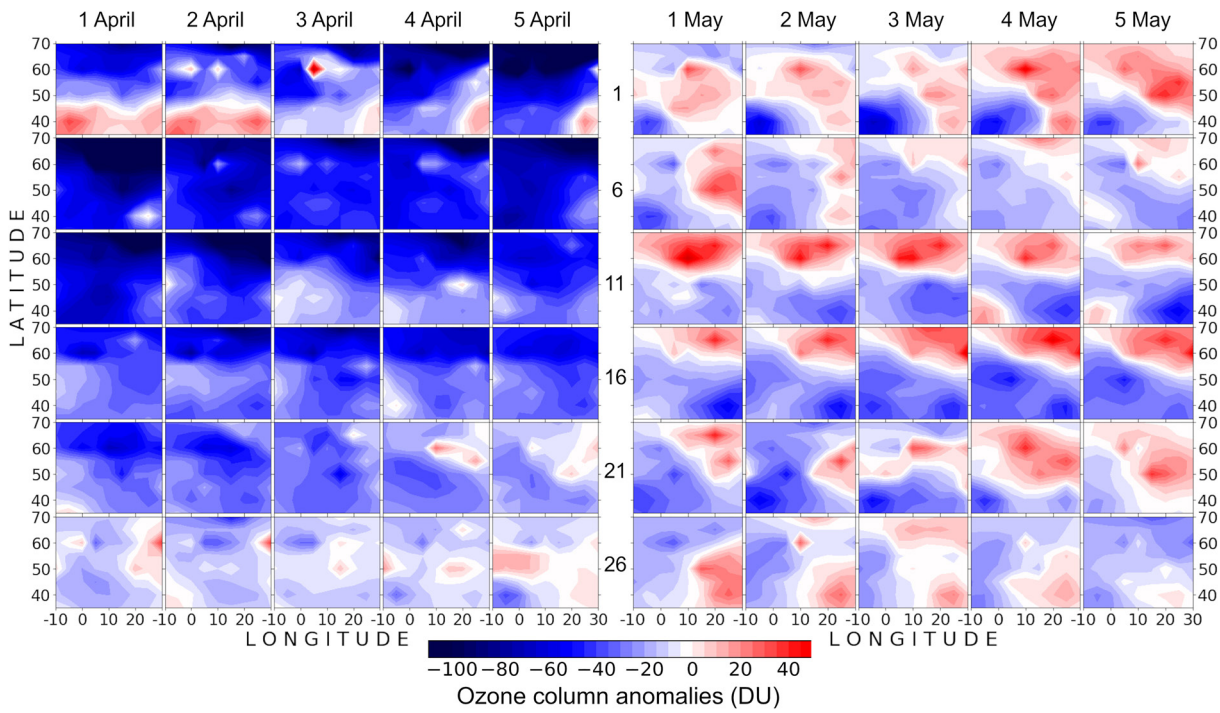


**Figure 6.** The distribution of the ozone column anomalies reconstructed over the European sector outlined in Figure 1 for April (left graph) and May (on the right graph) 2020. Each panel represents the daily anomalies and the upper left panel in both graphs corresponds to 1 April/May followed by 2 April/May in the same row and so on until 5 April/May. The second row starts with 6 April/May and following this order, the lower right panel exhibits the ozone distribution on 30 April/May. Numbers between the two graphs give the day associated with the first panels in the corresponding rows for April and May. Anomaly rates are determined by the color scale in Dobson Units (1 DU = $10^{-3}$ atm. cm = $2.69\times10^{16}$ mol/cm$^2$).



21698996, 2023, 3, Downloaded from https://agupubs.onlinelibrary.wiley.com/doi/10.1029/2022JD037581 by CochraneItalia, Wiley Online Library on [31/01/2023]. See the Terms and Conditions (https://onlinelibrary.wiley.com/terms-and-conditions) on Wiley Online Library for rules of use; OA articles are governed by the applicable Creative Commons License

21698996, 2023, 3, Downloaded from https://agupubs.onlinelibrary.wiley.com/doi/10.1029/2022JD037581 by Cochraneltalia, Wiley Online Library on [31/01/2023]. See the Terms and Conditions (https://onlinelibrary.wiley.com/terms-and-conditions) on Wiley Online Library for rules of use; OA articles are governed by the applicable Creative Commons License

in coastal zones and Chişinău is close to the Carpathian Mountains and to the Black Sea. Figure 5 also presents the latitudinal tendency of $\tau_D(S)$ through a linear best fit.

The similarity between the relative ozone variations observed in the Arctic during the period of strong ozone depletion and the corresponding variations seen with gradually increasing delays southward allows a causal link to be made between the directly observed Arctic ozone depletion and reductions in the ozone column far to the south. While this effect weakens as it moves south, as Figures 3 and 5 indicate, it still remained detectible in the descent of the April minima in $R_{S,Y}(t_D)$ below the 2.5th-percentile level in Figure 2.

### 3.3. Distribution of the Variations in Ozone Column Over Central Europe During the Spring 2020

The above analysis dealt with the latitudinal features of the ozone column response in Europe to the Arctic depletion episode. To give a more general picture of the ozone behavior in Europe, the distribution of its variation was reconstructed over a sector bounded by longitudes 10°W and 30°E and latitudes 35°N and 70°N (shown in Figure 1). The sector was covered by a grid of 5° resolution in both latitude and longitude and the ozone column at each of the grid points was evaluated by applying the Shepard (1968) interpolation approach as was made by Petkov et al. (2014) for studying the effect of the 2011 Arctic phenomenon. Following the Shepard method, the daily ozone column $Q_{m,n,Y}(t_D)$ at the grid point $(m, n)$ placed at latitude $m$ and longitude $n$, is determined for year $Y$ as a weighted average:

$$Q_{m,n,Y}(t_D) = \frac{\sum_{s=1}^{N} Q_{S,Y}(t_D)\left(r_s^{m,n}\right)^{-2}}{\sum_{s=1}^{N}\left(r_s^{m,n}\right)^{-2}}, \quad (3)$$

where $N$ is the number of the stations considered in the present analysis, $Q_{S,Y}(t_D)$ is the daily value of the ozone column measured at the station $S$ identified by a corresponding number in the first column of Table 1 and $r_s^{m,n}$ is the mutual distance between the grid point $(m, n)$ and station $S$. This distance (in km) was determined by applying the Lambert (1942) formula to the World Geodetic System 1984 spheroid (WGS84, 2000). This interpolation approach was considered to provide reliable assessments taking into account relatively homogeneous covering of the European area by stations (see Figure 1) and high correlation distances of the ozone column (Bojkov & Fioletov, 1995).

Both ozone distributions of $Q_{m,n,2020}(t_D)$ for 2020 and climatological ozone columns $Q_{m,n}(t_D)$ were calculated through Equation 3. The second parameter was computed by inserting the median ozone amount $Q_S(t_D)$ defined for Equation 1 instead of $Q_{S,Y}(t_D)$. Maps of the ozone column anomalies $Q_{m,n,2020}(t_D) - Q_{m,n}(t_D)$ constructed for the sector given in Figure 1 and the days of April and May 2020 are shown in Figure 6. It is seen that an ozone-poor area started to penetrate from the north at the beginning of April 2020 and rapidly spread all over the remaining sector by 23 April. During this period, the ozone column was between 50 and sometimes more than 100 DU lower with respect to the climatological mean values. During the last days of April 2020, the ozone column came close to the average level but areas with low amounts—predominantly in the south—persisted also in May. In fact, Figure 5 shows a 15 to 20-day delay of ozone reduction at the stations below 50°N with respect to the Arctic and taking into account the end of the episode in Ny-Ålesund (about 5 May) indicated in Figure 2, it can be concluded that the similar end at mid-latitudes should occur in the second half of May. Hence, in terms of the considered approach, it could be assumed that the ozone decrease in southern Europe in May 2020 is an echo of the Arctic episode.

## 4. Comparison Between the 2011 and 2020 Arctic Ozone Depletions and Their Effect on Mid-Latitude Ozone

As pointed out in Section 1, the 2020 Arctic ozone depletion was preceded by several similar episodes, the last of which occurred in 2011. This section aims to outline the evolution of 2011 and 2020 Arctic vortices, to compare the strengths of ozone depletions caused by them and to compare the responses of ozone column in Europe to both Arctic episodes.

21698996, 2023, 3, Downloaded from https://agupubs.onlinelibrary.wiley.com/doi/10.1029/2022JD037581 by CochraneItalia, Wiley Online Library on [31/01/2023]. See the Terms and Conditions (https://onlinelibrary.wiley.com/terms-and-conditions) on Wiley Online Library for rules of use; OA articles are governed by the applicable Creative Commons License

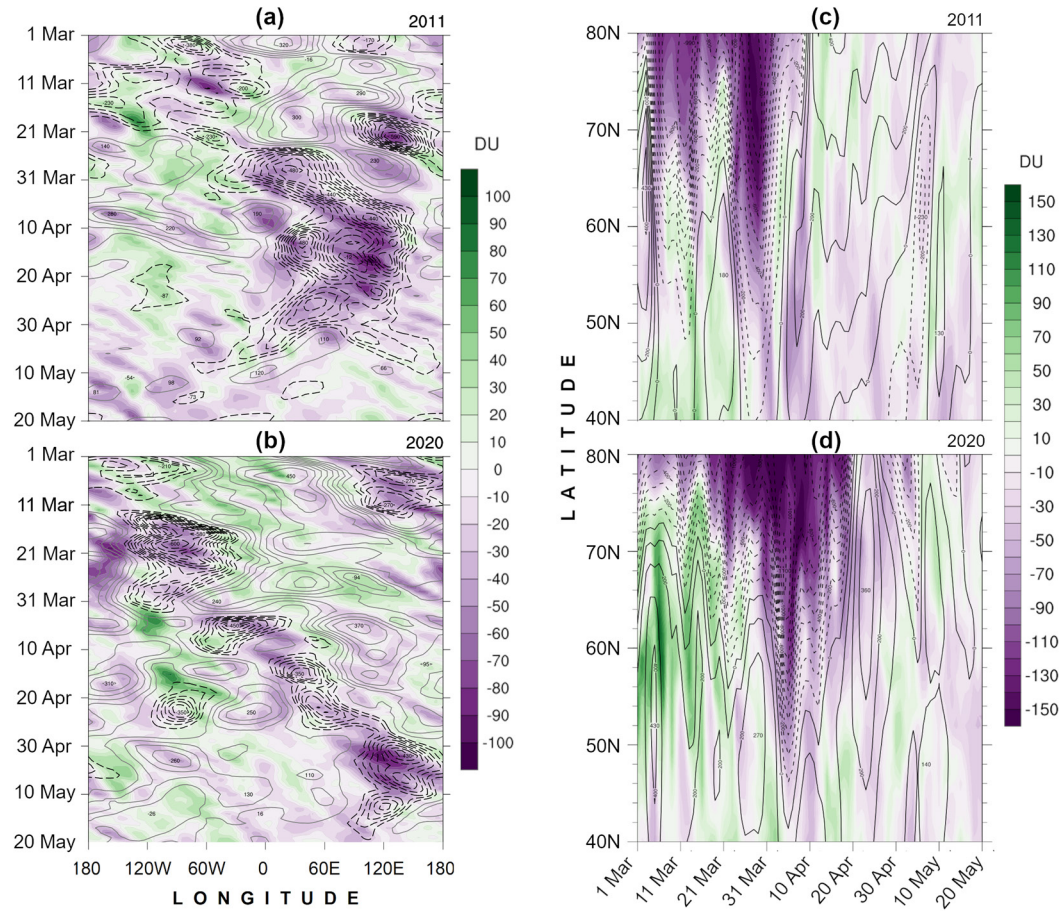


**Figure 7.** The first column represents the longitude-time Hovmöller diagrams of the ozone column anomalies evaluated by averaging over the 40°N–60°N latitude range and all longitudes for 2011 (a) and 2020 (b). The second column gives time-latitude diagrams for the anomalies estimated within 10°W–30°E longitude range for 2011 (c) and 2020 (d), respectively. In each panel the anomalies of geopotential height at 50 hPa level are also shown with dashed isolines for negative values and solid for the positive values indicated in both cases by the numbers.

### 4.1. Features of the 2011 and 2020 Polar Vortices and Behavior of Stratospheric Ozone

Since atmospheric dynamics is assumed to play an important role in Arctic ozone depletion episodes, dynamic processes are expected to have significant importance for the ozone distribution in the northern hemisphere after the breakup of the vortices. With that in mind, this section briefly reviews features of the Arctic stratospheric conditions in the springs of 2011 and 2020 according to the ERA-5 data set (ECMWF, 2021) by juxtaposing the distributions of anomalies in ozone column and geopotential height $Z$ at 50-hPa isobaric surface (Z50). The anomalies are referred to the 1981–2010 period. The second parameter was considered to represent the evolution of stratospheric polar vortex that is the main driver in the early spring stratosphere dynamics. The comparison was made by using Hovmöller diagrams (Hovmöller, 1949) computed for the 40°N–60°N latitude interval during the period from 1 March to 20 May for 2011 and 2020 (Figures 7a and 7b, respectively). Over Europe, this area includes most of the ozone measurement stations considered in this work and shown in Figure 1. Also, to complement the zonal evolution given by the Hovmöller diagrams, time-latitude diagrams were computed for the same period of 2011 (Figure 7c) and 2020 (Figure 7d) averaging the cprresponding fields on the 10°W–30°E longitudinal belt that corresponds to the selected sector in Figure 1. These diagrams show the meridional evolution from 80° to 40° N latitude over the European area of interest.

After a minor warming lasting for about one week at the beginning of February 2011, in March the polar vortex had largely recovered its strength and pole-centered position, resulting in a significant small-sizes vortex for the period (Kuttippurath et al., 2012). In this phase, the temperature was unusually low (Hurwitz et al., 2011), enough to form polar stratospheric clouds and, as a result, to cause a severe ozone loss (Pommereau et al., 2013). Also,

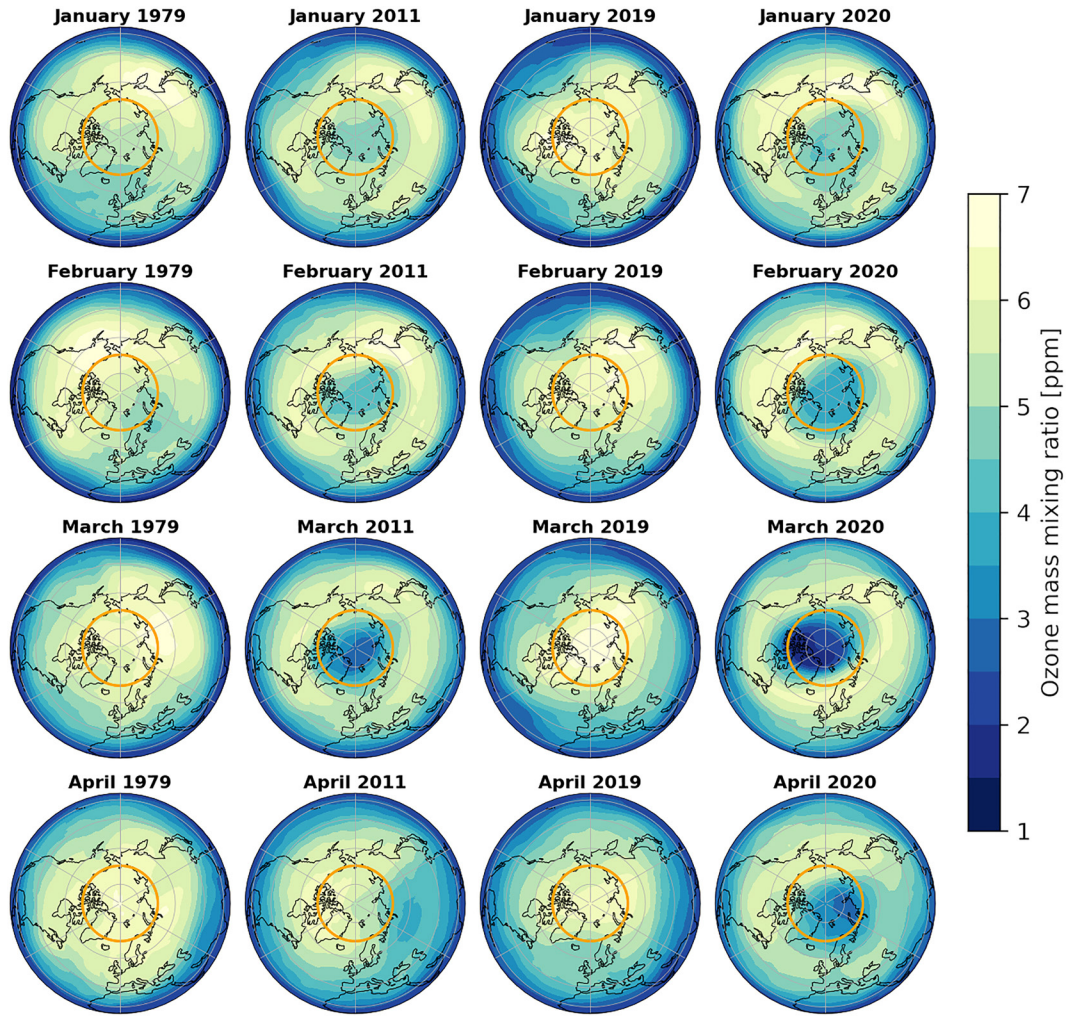


**Figure 8.** Distribution of the monthly mean ozone mass mixing ratio $\rho_{O3}(\varphi, \lambda, M, Y)$ in the northern hemisphere at 50 hPa altitude level for January–April of 1979, 2011, 2019, and 2020, respectively. The orange circles indicate the 70°N latitude.

the vortex strengthening during February-March limited the dynamical dilution with higher-ozone extra-vortex air masses, reinforcing the feedback between cold temperatures and chemical ozone depletion in the following weeks (Hu & Xia, 2013; Manney et al., 2011).

Although the vortex underwent little deformation, in the second half of March 2011 it started to migrate from the Arctic to the Siberian mid-latitudes where it dissipated after the final warming in April. Figure 7a shows that a predominant signature of the vortex appears over Europe, south of 60°N, during the last third of March: a wide area of negative Z50 anomalies is co-located with a negative ozone column anomaly that peaks over central-western Europe. As shown in Figure 7c, during that period this area was affected by a southward advection of low-ozone airmasses whose minimum values reached a latitude of 40°N between 31 March and the first days of April. This result is consistent with the observational data recorded at Madrid and Rome shown in Figure 2. Although the main negative Z50 anomaly shifted eastward in the following days, as seen in Figure 7a, low values of ozone concentration still affected Western Europe at the beginning of April, while Z50 exhibited weak positive anomalies (see for instance the Madrid station in Figure 2a). This indicates that, despite the shorter-scale dynamical evolution, the whole region was still influenced by the polar vortex during its slow move toward Eurasia: specifically, being affected by the southward advected component of the large-scale circulation of low-ozone airmasses.

Turning to the 2019/2020 event, here the polar vortex showed remarkable characteristics from its earliest formation: for instance, this strong, stable and cold polar vortex featured the lowest minimum 50-hPa temperatures



21698996, 2023, 3, Downloaded from https://agupubs.onlinelibrary.wiley.com/doi/10.1029/2022JD037581 by CochraneItalia, Wiley Online Library on [31/01/2023]. See the Terms and Conditions (https://onlinelibrary.wiley.com/terms-and-conditions) on Wiley Online Library for rules of use; OA articles are governed by the applicable Creative Commons License

21698996, 2023, 3, Downloaded from https://agupubs.onlinelibrary.wiley.com/doi/10.1029/2022JD037581 by CochraneItalia, Wiley Online Library on [31/01/2023]. See the Terms and Conditions (https://onlinelibrary.wiley.com/terms-and-conditions) on Wiley Online Library for rules of use; OA articles are governed by the applicable Creative Commons License

in the polar cap (north of 50°N latitude) from the beginning of December to the end of March (e.g., Dameris et al., 2021). The polar vortex remained nearly undisturbed also because of the weak tropospheric wave activity in most of the 2019/2020 winter, with no warming or significant deformations taking place (Lawrence et al., 2020). However, in early March, the stratospheric vortex was slightly displaced and it started to be observable at lower latitudes. Figure 7b shows the main negative anomalies of Z50 and ozone column moving during the first 2 weeks of March from the Northern Pacific to the Canadian region, where this lobe of the vortex persisted until the end of the month, consistent with the observations performed in the Canadian sector of the Arctic (Bognar et al., 2021). In the following days, the vortex shifted to the east directly affecting Europe during the first half of April. In this early spring period, the abrupt record-breaking loss of polar cap ozone column was observed (Lawrence et al., 2020; Wohltmann et al., 2020). Figure 7d shows that the lowest ozone column values initially affected Europe within the southward shift of the vortex (negative Z50 anomaly), touching the 40°N latitude areas in the first days of April, as confirmed from the ground-based measurements (Figures 2 and 6). As for the 2011 episode, this outcome is consistent, for instance, with Madrid observational data shown in Figure 2a. Afterward, although the negative Z50 anomalies were more active over Eastern Europe, low ozone airmasses associated to the vortex lobe affected the European domain of Figure 7b until approximately 25 April. In the following period the European lobe of the polar vortex exhibited a clear move toward the eastern hemisphere, slowly dissipating in May.

Overall, the Hovmöller diagrams for the two major events in 2011 and 2020 show the influence of a strong polar vortex exhibited as Z50 and ozone column negative anomalies that extends over both a large spatial scale and persists for a long time. Due to a slight displacement of the vortex or to the slow transit of a vortex lobe, during both years, low ozone values can also be observed at southern latitudes (40°N). However, as indicated by the time-latitude diagrams, the evolution of the ozone minima shows greater variability consistent with shorter time-space scales as it travels southward. It can be assumed that this enhanced variability causes the higher dispersion of the delays $\tau_D(S)$ determined for lower latitudes in Figure 5 especially in 2011. The meridional difference in the scale of the ozone fluctuations suggests that at northern latitudes the vortex acts as a slow-moving reservoir of low-ozone airmass. This reservoir is partially eroded by fast-moving, synoptic-scale atmospheric systems that advect low-ozone air masses at southern latitudes.

Before comparing the responses of the ozone column over Europe to the 2011 and 2020 Arctic ozone depletions, the strength of both events is discussed in the next subsection.

### 4.2. Stratospheric Ozone Depletion Depths Reached in Past Events

The data provided by ERA-5 reanalyses (ECMWF, 2021) that cover a 42-year period, from 1979 to 2020 were considered in this section and the brief survey below is focused on the lower stratosphere, which contains the majority of the columnar ozone (Brasseur & Solomon, 2005).

Specifically, we consider the ERA-5 ozone mass mixing ratio at 100 hPa that corresponds approximately to 16 km a.s.l., 50 hPa (∼ 19 km) and 30 hPa (∼ 22 km). Since the frequent changes in intensity and shape of the Arctic vortex is reflected in ozone depletion, it was likewise assumed that the monthly means of the ozone mass mixing ratio $\rho_{O3}$, which smooth the short-term variations, can provide a realistic picture of the seasonal ozone evolution. Figure 8 exhibits some example distributions of $\rho_{O3}(\varphi, \lambda, M, Y)$ defined at latitude $\varphi$ and longitude $\lambda$ of the northern hemisphere, for month $M$ of the year $Y$. The distributions are shown for the 50 hPa altitude level. The profound ozone depletion episodes that occurred in 2011 and 2020 can be recognised in Figure 8. The areas characterized by appreciably low ozone content in terms of monthly averaged $\rho_{O3}(\varphi, \lambda, M, Y)$ lie close to the North Pole and the majority is bounded by the 70°N circle of latitude. For that reason, the next step of the parametrization was calculation of the zonal mean values $\rho_{O3}(M, Y)$ for $\varphi \geq 70°$N and $-180° < \lambda \leq 180°$. Such an approach was assumed to provide a fair representation of the monthly status of ozone in the Arctic; the result is a time series that describes the ozone evolution at the 50 hPa altitude level in the Arctic during the considered 42-year period. Similarly, the time patterns of $\rho_{O3}(M, Y)$ were evaluated also for the 100 hPa and 30 hPa levels. The lowest value $\rho_{min}(Y)$ of $\rho_{O3}(M, Y)$ in the February–April period was then taken for each year and Figure 9 shows the variations of these minima. The median of the $\rho_{\min}(Y)$ values are also indicated in each panel together with the fifteenth percentile. It can be seen that $\rho_{\min}(Y)$ occasionally dropped below the fifteenth percentile after the middle of the 1990s while for 1997, 2011, and 2020 such a decrease occurred at all three selected altitudes.

It should be pointed that the $\rho_{\min}(Y)$ time series at 50 hPa and 100 hPa altitude levels given in Figure 9 show good agreement with the time dependence of the February–April mean ozone column evaluated by Lawrence

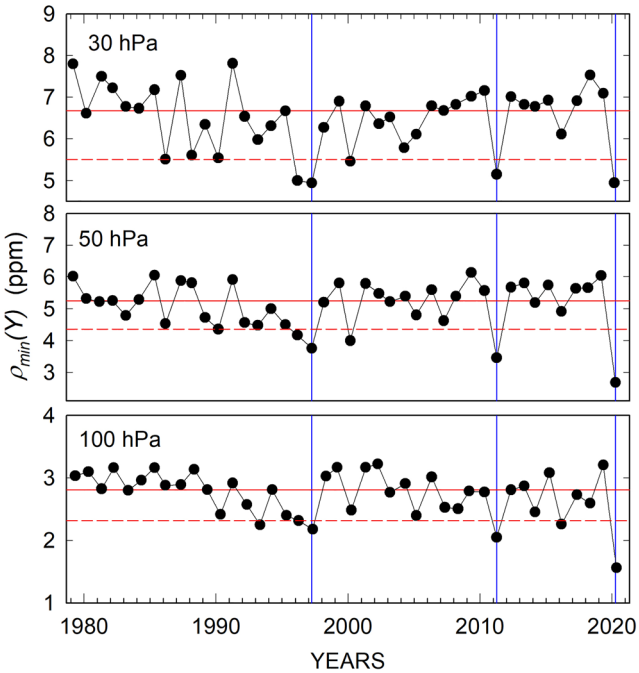


**Figure 9.** Time patterns of the February–April minima $\rho_{\min}(Y)$ of $\rho_{O3}(M, Y)$ for the three considered altitude levels given in the panels. The red solid and dashed lines in each of the panels represent the median of $\rho_{\min}(Y)$ and the fifteenth percentile, respectively. The vertical blue lines indicate March of 1997, 2011, and 2020.

et al. (2020, their Figure 12) and the March mean values obtained by Inness et al. (2020, their Figure 1) both assessed for the Arctic from 1979 to 2020. Figure 9 shows that in 2020 the ozone minimum $\rho_{\min}(Y)$ was the deepest at lower stratosphere levels especially at 100 hPa, consistent with the findings of Manney et al. (2020). Generally speaking, Figure 9 indicates that the 2020 depletion event is by far the strongest in the 42-year record which is consistent with the reults of other researches.

### 4.3. Comparison of the Ozone Column Responses in Europe to the 2011 and 2020 Arctic Episodes

The response of the mid-latitude European ozone column to the 2011 Arctic ozone depletion event was examined by Petkov et al. (2014). The main results of this analysis were presented in Figures 2, 3 and 5 through the same parameterization adopted in the present work in order to draw a parallel between 2011 and 2020 phenomena. Figure 2 exhibits the behavior of ratios $R_{S,2011}(t_D)$ evaluated for the corresponding sites in the same months as for $R_{S,2020}(t_D)$. An apparent similarity can be noted between the evolution of ozone column observed in spring of both 2011 and 2020. The ozone recovering phases in both $R_{S,2011}(t_D)$ and $R_{S,2020}(t_D)$ were comparable to each other at more of the lower-latitude stations. The magnitudes of ozone reductions $Q_{\min}(S)$ and the delays in the ozone response to the Arctic episode $\tau_D(S)$ registered at all stations were found to be similar as illustrated by Figures 3 and 5. It was found that $Q_{\min}(S)$ was decreased from 80°N to 40°N by approximately 0.7% deg$^{-1}$ in 2020 and 2011 (see Figure 3). The gradients of the corresponding delays $\tau_D(S)$ are $0.59 \pm 0.06\%$ deg$^{-1}$ in 2020 and $0.48 \pm 0.01\%$ deg$^{-1}$ in 2011, values differ from each other by about 8% at the 1 $\sigma$ level.

At the same time, Figure 2 shows an earlier start of the $R_{S,2011}(t_D)$ decrease and earlier appearance of the $R_{S,2011}(t_D)$ minima with respect to the $R_{S,2020}(t_D)$ minima with a more pronounced onset at the northern sites in 2020. Another important difference between 2011 and 2020 episodes was the shorter duration of the periods with reduced ozone column in 2011. These differences can be seen also in Figures 7c and 7d that represent the ozone evolution in the considered latitudes and were discussed in the previous subsection. According to Figure 7c the ozone decrease at 80°N, that is close to the latitude of Ny-Ålesund station, started at the beginning of March 2011 and reached the lowest value at the end of March persisting for a few days before recovering. In 2020 (Figure 7d), after slight fluctuations, the ozone started to decrease from the middle of March and reached its minimum at the end of the month remaining at this level until the second half of April. These behaviors of the ozone column in the springtime of 2011 and 2020 are similar to the corresponding ones depicted by the ground-based measurements and presented in the Ny-Ålesund panel of Figure 2a.

Figure 7c indicates that the ozone depleted airmasses in 2011 covered with slight variations the European areas from 80°N to about 65°N for approximately the same period. This occurrence is represented by the same almost zero delay $\tau_D(S)$ for this latitudinal range in Figure 5. Below 60°N the ozone started to decrease in late March, or 15–20 days after its initial decrease time at 80°N (Figure 7c) that is also in consistent with the sharply increased delays in Figure 5. The analogous start of the ozone decrease episode in 2020 (Figure 7d) smoothly moved from the middle of March at 80°N to early April at about 40°N resulting in a gradually increasing delay from a few days at 70°N to about 20 days at 40°N (Figure 5).

Figure 7d indicates that the anomalies averaged over 10°W and 30°E are predominantly negative below 50°N in late April and May 2020. These features correspond to the ozone distributions shown in Figure 6, where low ozone regions in southern Europe can be noted in May 2020. According to the discussion in Section 4.1 it should be pointed out the presence of the vortex lobe to the east of the sector that persisted until the second half of May 2020 (Figure 7b). This occurrence supports the hypothesis made at the end of Section 3.3 based on ground observations that the minima of the ozone column in the southern Europe registered in May 2020 is an echo of the Arctic phenomenon.



21698996, 2023, 3, Downloaded from https://agupubs.onlinelibrary.wiley.com/doi/10.1029/2022JD037581 by Cochraneltalia, Wiley Online Library on [31/01/2023]. See the Terms and Conditions (https://onlinelibrary.wiley.com/terms-and-conditions) on Wiley Online Library for rules of use; OA articles are governed by the applicable Creative Commons License

21698996, 2023, 3, Downloaded from https://agupubs.onlinelibrary.wiley.com/doi/10.1029/2022JD037581 by CochraneItalia, Wiley Online Library on [31/01/2023]. See the Terms and Conditions (https://onlinelibrary.wiley.com/terms-and-conditions) on Wiley Online Library for rules of use; OA articles are governed by the applicable Creative Commons License

Summarizing, it can be noted that despite some differences in the development and strength of the 2011 and 2020 ozone depletion episodes in the Arctic, both led to generally similar effects on the ozone over mid-latitude European areas.

## 5. Conclusions

The impact of the Arctic ozone depletion episode that occurred in spring 2020 on the ozone column at lower latitudes across Europe was studied by examining the ground observations predominantly performed by Brewer and Dobson spectrophotometers at 38 stations located from the Arctic to nearly 40°N. The ozone loss was assessed relative to the climatological mean at each station and timepoint for the first half of 2020. At the northernmost station Ny-Ålesund (79°N) the decrease of the ozone column started in the middle of March, reached an amount of about 43% lower than expected values in the first days of April, and this lasted about two weeks. The final recovery of the ozone to within climatological norms occurred at the beginning of May and the progress of the relative variations observed at the other sites were compared with that at Ny-Ålesund. Deep ozone column minima that appeared at the stations below the polar circle during the period of the Arctic episode were also observed and their deepness gradually declined to about 15% at 40°N. The unusual decrease in mid-latitude ozone column in April and May, when the solar elevation rapidly increases can lead to an increase in solar ultraviolet radiation at the ground that has important health consequences in the densely populated European regions as noted in Section 3.1.

The temporal evolution of the ozone column decrease at lower latitude stations was similar to that at Ny-Ålesund but it occurred with a delay of between 1 to nearly 20 days moving south. These findings imply a causal relationship between ozone depletion in the Arctic and at lower latitudes. A similar response of the mid-latitude ozone was observed in 2011 after the corresponding Arctic ozone depletion. To better understand these responses, stratospheric dynamical patterns in 2011 and 2020 were examined by constructing Hovmöller diagrams for the March-May period of each year. In both cases a migration of the ozone-poor air masses from the Arctic southward was found to be the main reason of the observed ozone decreases in Southern Europe. Short scale structures in the distribution of ozone anomalies at the southernmost latitudes in the Hovmöller diagrams, suggests that short scale systems steer the meridional advection far from the vortex core.

Despite differences in the strength of 2011 and 2020 episodes, and differences in their evolution, the response of the mid-latitude ozone column was quite similar in both cases. Taking into account the role of atmospheric ozone in protection of the life on the Earth, the analysis in the present work highlights the importance of ozone layer monitoring in a changing climate.

## Data Availability Statement

Total ozone column data from ground stations used to study the response of the ozone over Europe to the 2020 Arctic ozone depletion are freely available at the World Ozone and Ultraviolet Data Centre (WOUDC, 2020); data from SAOZ (2020) spectrometers were also used. The GUV time series for Ny-Ålesund was provided by Svendby (2021), while the data from UV-RAD at the same station can be accessed at Exaodep-2020 (2021). Data of ozone column for the stations Trondheim and Bergen were provided by Johnsen (2022) and data for Stara Zagora by Werner (2022). ERA-5 reanalysis data were used for the study of the ozone behaviour at the three selected stratospheric levels and for construction of the Hovmöller diagrams (ECMWF (2021)). These diagrams were made by means of the NCAR Command Language NCL (2019). The map and underlying data at Figure 1 was created using ArcGIS® software by Esri (2019).

**Acknowledgments**
The authors gratefully acknowledge the World Ozone and Ultraviolet Radiation Data Centre (WOUDC) for providing the data set of ground-based measured ozone column, and all organisations responsible for each of the stations used here, which afford their data to WOUDC, making this study possible. The European Centre for Medium-Range Weather Forecasts (ECMWF) is also acknowledged for providing data about stratospheric ozone content and potential vorticity. The authors thank anonymous reviewers for their constructive and valuable comments. The participation of Kamil Láska in this work was funded by the Ministry of Education, Youth and Sports of the Czech Republic, No. VAN 2022. The study was partially supported by the RadiCa Project in framework of the Italian National Research Program in Antarctica (PNRA).

## References

Arnone, E., Castelli, E., Papandrea, E., Carlotti, M., & Dinelli, B. M. (2012). Extreme ozone depletion in the 2010–2011 Arctic winter stratosphere as observed by MIPAS/ENVISAT using a 2-D tomographic approach. *Atmospheric Chemistry and Physics*, *12*, 9149–9165. https://doi.org/10.5194/acp-12-9149-2012

Bernhard, G., Fioletov, V. E., Grooß, J.-U., Ialongo, I., Johnsen, B., Lakkala, K., et al. (2020). Record-breaking increases in arctic solar ultraviolet radiation caused by exceptionally large ozone depletion in 2020. *Geophysical Research Letters*, *47*(24). https://doi.org/10.1029/2020GL090844

Bognar, K., Alwarda, R., Strong, K., Chipperfield, M. P., Dhomse, S. S., Drummond, J. R., et al. (2021). Unprecedented spring 2020 ozone depletion in the context of 20 years of measurements at Eureka, Canada. *Journal Geophysical Research Atmosphere*, *126*, e2020JD034365. https://doi.org/10.1029/2020jd034365

Bojkov, R. D., & Fioletov, V. E. (1995). Estimating the global ozone characteristics during the last 30 years. *Journal of Geophysical Researches*, *100*(D8), 16537–16551. https://doi.org/10.1029/95jd00692

Brasseur, G. P., & Solomon, S. (2005). *Aeronomy of the middle atmosphere* (pp. 443–531). Springer.

Chipperfield, M. P., & Jones, R. L. (1999). Relative influences of atmospheric chemistry and transport on arctic ozone trends. *Nature*, *400*, 551–554. https://doi.org/10.1038/22999

Coy, L., Nash, E. R., & Newman, P. A. (1997). Meteorology of the polar vortex: Spring 1997. *Geophysical Research Letters*, *24*(22), 2693–2696. https://doi.org/10.1029/97gl52832

Crutzen, P. J., & Arnold, F. (1986). Nitric acid cloud formation in the cold Antarctic stratosphere: A major cause for the springtime' ozone hole. *Nature*, *324*, 651–655. https://doi.org/10.1038/324651a0

Dameris, M., Loyola, D. G., Nützel, M., Coldewey-Egbers, M., Lerot, C., Romahn, F., & Van Roozendael, M. (2021). Record low ozone values over the Arctic in boreal spring 2020. *Atmospheric Chemistry and Physics*, *21*, 617–633. https://doi.org/10.5194/acp-21-617-2021

ECMWF. (2021). European centre for medium-range weather forecasts, ERA-5 reanalyses [Registration required]. https://doi.org/10.24381/cds.adbb2d47

Esri (2019). ArcGIS geographic information system software [Software], Retrieved from www.esri.com/software/arcgis

Exaodep-2020 (2021). EXAODEP-2020 ozone column at Ny-Alesund Svalbard station, Italian Arctic data center (IADC). Retrieved from https://data.iadc.cnr.it/erddap/files/ozone-ny-alesund/

Farman, J. C., Gardiner, B. G., & Shanklin, J. D. (1985). Large losses of total ozone in Antarctica reveal seasonal C1Ox/NOx interaction. *Nature*, *315*, 207–210. https://doi.org/10.1038/315207a0

Gröbner, J., Schill, H., Egli, L., & Stübi, R. (2021). Consistency of total column ozone measurements between the Brewer and Dobson spectroradiometers of the LKO Arosa and PMOD/WRC Davos. *Atmospheric Measurement Techniques*, *14*, 3319–3331. https://doi.org/10.5194/amt-14-3319-2021

Harris, N. R. P., Lehmann, R., Rex, M., & Von Der Gathen, P. (2010). A closer look at Arctic ozone loss and polar stratospheric clouds. *Atmospheric Chemistry and Physics*, *10*, 8499–8510. https://doi.org/10.5194/acp-10-8499-2010

Hauchecorne, A., Godin, S., Marchand, M., Hesse, B., & Souprayen, C. (2002). Quantification of the transport of chemical constituents from the polar vortex to midlatitudes in the lower stratosphere using the high-resolution advection model MIMOSA and effective diffusivity. *Journal of Geophysical Research*, *107*(D20), 8289. https://doi.org/10.1029/2001JD000491

Hovmöller, E. (1949). The trough-and-ridge diagram. *Tellus*, 1, 62–66. https://doi.org/10.1111/j.2153-3490.1949.tb01260.x

Hu, Y. Y., & Xia, Y. (2013). Extremely cold and persistent stratospheric arctic vortex in the winter of 2010–2011. *Chinese Science Bulletin*, *58*(25), 3155–3160. https://doi.org/10.1007/s11434-013-5945-5

Hurwitz, M. M., Newman, P. A., & Garfinkel, C. I. (2011). The Arctic vortex in March 2011: A dynamical perspective. *Atmospheric Chemistry and Physics*, *11*, 11447–11453. https://doi.org/10.5194/acp-11-11447-2011

Inness, A., Chabrillat, S., Flemming, J., Huijnen, V., Langenrock, B., Nicolas, J., et al. (2020). Exceptionally low Arctic stratospheric ozone in spring 2020 as seen in the CAMS reanalysis. *Journal of Geophysical Research: Atmospheres*, *125*, e2020JD033563. https://doi.org/10.1029/2020JD033563

Isaksen, I. S. A., Zerefos, C., Wang, W.-C., Balis, D., Eleftheratos, K., Rognerud, B., et al. (2012). Attribution of the Arctic ozone column deficit in March 2011. *Geophysical Research Letters*, *39*, L24810. https://doi.org/10.1029/2012GL053876

Johnsen, B. (2022). Ozone_CLT. Retrieved from https://github.com/uvnrpa/Ozone_CLT

Knudsen, B. M., & Grooß, J.-U. (2000). Northern midlatitude stratospheric ozone dilution in spring modelled with simulated mixing. *Journal of Geophysical Research*, *105*, 6885–6890. https://doi.org/10.1029/1999jd901076

Koch, G., Wernli, H., Buss, S., Staehelin, J., Peter, T., Liniger, M. A., & Meilinger, S. (2004). Quantification of the impact in mid-latitudes of chemical ozone depletion in the 1999/2000 arctic polar vortex prior to the vortex breakup. *Atmospheric Chemistry and Physics Discussions*, *4*, 1911–1940.

Koukouli, M. E., Lerot, C., Granville, J., Goutail, F., Lambert, J.-C., Pommereau, J.-P., et al. (2015). Evaluating a new homogeneous total ozone climate data record from GOME/ERS-2, SCIAMACHY/Envisat, and GOME-2/MetOp-A. *Journal of Geophysical Research: Atmosphere*, *120*, 12296–12312. https://doi.org/10.1002/2015JD023699

Kuttippurath, J., Godin-Beekmann, S., Lefèvre, F., Nikulin, G., Santee, M. L., & Froidevaux, L. (2012). Record-breaking ozone loss in the arctic winter 2010/2011: Comparison with 1996/1997. *Atmospheric Chemistry and Physics*, *12*, 7073–7085. https://doi.org/10.5194/acp-12-7073-2012

Lambert, W. D. (1942). The distance between two widely separated points on the Earth surface. *Journal of the Washington Academy of Sciences*, *32*, 125–130.

Lawrence, Z. D., Perlwitz, J., Butler, A. H., Manney, G. L., Newman, P. A., Lee, S. H., & Nash, E. R. (2020). The remarkably strong arctic stratospheric polar vortex of winter 2020: Links to record-breaking arctic oscillation and ozone loss. *Journal of Geophysical Research*, *125*(22). https://doi.org/10.1029/2020JD033271

Manney, G. L., Livesey, N. J., Santee, M. L., Froidevaux, L., Lambert, A., Lawrence, Z. D., et al. (2020). Record-low Arctic stratospheric ozone in 2020: MLS observations of chemical processes and comparisons with previous extreme winters. *Geophysical Research Letters*, *47*, e2020GL089063. https://doi.org/10.1029/2020GL089063

Manney, G. L., Santee, M. L., Rex, M., Livesey, N. J., Pitts, M. C., Veefkind, P., et al. (2011). Unprecedented arctic ozone loss in 2011. *Nature*, *478*, 469–475. https://doi.org/10.1038/nature10556

Manney, G. L., Zurek, R. W., Gelman, M. E., Miller, A. J., & Nagatani, R. (1994). The anomalous arctic lower stratospheric polar vortex of 1992–1993. *Geophysical Research Letters*, *21*, 2405–2408. https://doi.org/10.1029/94gl02368

Molina, M. J., & Rowland, F. S. (1974). Stratospheric sink for chlorofluoromethanes: Chlorine atom catalysed destruction of ozone. *Nature*, *249*, 810–812. https://doi.org/10.1038/249810a0

Morys, M., Mims, F. M., III, Hagerup, S., Anderson, S. E., Baker, A., Kia, J., & Walkup, T. (2001). Design, calibration, and performance of MICROTOPS II handheld ozone monitor and sun photometer. *Journal of Geophysical Research*, *106*, 14573–14582. https://doi.org/10.1029/2001jd900103

NCL (2019). The NCAR command language (Version 6.6.2) [Software]. UCAR/NCAR/CISL/TDD. https://doi.org/10.5065/D6WD3XH5

Nerobelov, G., Timofeyev, Y., Virolainen, Y., Polyakov, A., Solomatnikova, A., Poberovskii, A., et al. (2022). Measurements and modelling of total ozone columns near St. Petersburg, Russia. *Remote Sensing*, *14*, 3944. https://doi.org/10.3390/rs14163944

Petkov, B., Vitale, V., Di Carlo, P., Mazzola, M., Lupi, A., Diémoz, H., et al. (2021). The 2020 arctic ozone depletion and signs of its effect on the ozone column at lower latitudes. *Bulletin of Atmospheric Science and Technology*, *2*, 8. https://doi.org/10.1007/s42865-021-00040-x

Petkov, B., Vitale, V., Tomasi, C., Bonafé, U., Scaglione, S., Flori, D., et al. (2006). Narrow-band filter radiometer for ground-based measurements of global UV solar irradiance and total ozone. *Applied Optics*, *45*(18), 4383–4395. https://doi.org/10.1364/ao.45.004383



21698996, 2023, 3, Downloaded from https://agupubs.onlinelibrary.wiley.com/doi/10.1029/2022JD037581 by Cochraneltalia, Wiley Online Library on [31/01/2023]. See the Terms and Conditions (https://onlinelibrary.wiley.com/terms-and-conditions) on Wiley Online Library for rules of use; OA articles are governed by the applicable Creative Commons License

Petkov, B. H., Vitale, V., Hansen, G. H., Svendby, T. M., Sobolewski, P. S., Láska, K., et al. (2019). Observations of the solar UV irradiance and ozone column at Svalbard. In Orr, et al. (eds) *SESS report 2018, svalbard integrated arctic Earth observing system, Longyearbyen*, 170–183. Retrieved from https://sios-svalbard.org/SESS_Issue1

Petkov, B. H., Vitale, V., Tomasi, C., Siani, A. M., Seckmeyer, G., Webb, A. R., et al. (2014). Response of the ozone column over Europe to the 2011 arctic ozone depletion event according to ground-based observations and assessment of the consequent variations in surface UV irradiance. *Atmospheric Environment*, *85*, 169–178. https://doi.org/10.1016/j.atmosenv.2013.12.005

Pommereau, J. P., & Goutail, F. (1988). Ozone and $NO_2$ ground-based measurements by visible spectrometry during Arctic winter and spring 1988. *Geophysical Research Letters*, *15*, 891–894. https://doi.org/10.1029/GL015i008p00891

Pommereau, J.-P., Goutail, F., Lefèvre, F., Pazmino, A., Adams, C., Dorokhov, V., et al. (2013). Why unprecedented ozone loss in the Arctic in 2011? Is it related to climate change? *Atmospheric Chemistry and Physics*, *13*, 5299–5308. https://doi.org/10.5194/acp-13-5299-2013

Rösevall, J. D., Murtagh, D. P., Urban, J., Feng, W., Eriksson, P., & Brohede, S. (2008). A study of ozone depletion in the 2004/2005 Arctic winter based on data from Odin/SMR and Aura/MLS. *Journal of Geophysical Research*, *113*, D13301. https://doi.org/10.1029/2007JD009560

SAOZ (2020). Systeme d'Analyse par observation zenitale, Consolidated data V3, Retrieved from http://saoz.obs.uvsq.fr/SAOZ_consol_v3.html

Shepard, D. A. (1968). *A two-dimensional interpolation function for irregularly-spaced data*. Proceedings of 1968 23rd ACM National Conference, 517–524. https://doi.org/10.1145/800186.810616

Solomon, S., Haskins, J., Ivy, D. J., & Min, F. (2014). Fundamental differences between Arctic and Antarctic ozone depletion. *Proceedings of the National Academy of Sciences*, *111*, 6220–6225. https://doi.org/10.1073/pnas.1319307111

Solomon, S., Portmann, R. W., & Thompson, D. W. J. (2007). Contrasts between Antarctic and Arctic ozone depletion. *Proceedings of the National Academy of Sciences*, *104*(2), 445–449. https://doi.org/10.1073/pnas.0604895104

Strahan, S. E., Douglass, A. R., & Newman, P. A. (2013). The contributions of chemistry and transport to low arctic ozone in March 2011 derived from AuraMLS observations. *Journal of Geophysical Researches: Atmosphere*, *118*, 1563–1576. https://doi.org/10.1002/jgrd.50181

Strahan, S. E., Douglass, A. R., & Steenrod, S. D. (2016). Chemical and dynamical impacts of stratospheric sudden warmings on arctic ozone variability. *Journal of Geophysical Research: Atmosphere*, *121*, 11836–11851. https://doi.org/10.1002/2016JD025128

Svendby, T. M. (2021). GUV total ozone column and effective cloud transmittance from three Norwegian sites 1995-2019 (v1.0). Zenodo. https://doi.org/10.5281/zenodo.4446609

Svendby, T. M., Johnsen, B., Kylling, A., Dahlback, A., Bernhard, G. H., Hansen, G. H., et al. (2021). GUV long-term measurements of total ozone column and effective cloud transmittance at three Norwegian sites. *Atmospheric Chemistry and Physics*, *21*, 7881–7899. https://doi.org/10.5194/acp-21-7881-2021

Tegtmeier, S., Rex, M., Wohltmann, I., & Krüger, K. (2008). Relative importance of dynamical and chemical contributions to arctic wintertime ozone. *Geophysical Research Letters*, *35*, L17801. https://doi.org/10.1029/2008GL034250

Tilmes, S., Müller, R., Engel, A., Rex, M., & Russell, J. M., III. (2006). Chemical ozone loss in the Arctic and Antarctic stratosphere between 1992 and 2005. *Geophysical Research Letters*, *33*, L20812. https://doi.org/10.1029/2006GL026925

Von der Gathen, P., Kivi, R., Wohltmann, I., Salawitch, R. J., & Rex, M. (2021). Climate change favours large seasonal loss of arctic ozone. *Nature Communications*, *12*, 3886. https://doi.org/10.1038/s41467-021-24089-6

Werner, R. (2022). GUV total ozone column from Stara Zagora, Bulgaria, 2015–2021. https://tracegases.nuclearmodels.net/Ozone/

WGS84 (2000). *World geodetic system 1984*. Department of Defense, National Imagery and Mapping Agency Technical Report TR8350.

Whaley, C., Strong, K., Adams, C., Bourassa, A. E., Daffer, W. H., Degenstein, D. A., et al. (2013). Using FTIR measurements of stratospheric composition to identify mid-latitude polar vortex intrusions over Toronto. *Journal of Geophysicl Research Atmosphere*, *118*, 12766–12783. https://doi.org/10.1002/2013JD020577

WMO (2007). *Scientific assessment of ozone depletion: 2006. Global ozone research and monitoring project—rep. 50*. World Meteorological Organization.

WMO (2010). *Scientific assessment of ozone depletion: 2010*. World Meteorological Organization Report No. 52, World Meteorological Organization.

WMO (2018). *Scientific assessment of ozone depletion: 2018, chapter 4*. Global Ozone Research and Monitoring Project Report No. 58.

Wohltmann, I., Von Der Gathen, P., Lehmann, R., Maturilli, M., Deckelmann, H., Manney, G. L., et al. (2020). Near-complete local reduction of arctic stratospheric ozone by severe chemical loss in spring 2020. *Geophysical Research Letters*, *47*, e2020GL089547. https://doi.org/10.1029/2020GL089547

WOUDC (2020). World ozone and ultraviolet data centre. https://doi.org/10.14287/10000001



21698996, 2023, 3, Downloaded from https://agupubs.onlinelibrary.wiley.com/doi/10.1029/2022JD037581 by Cochraneltalia, Wiley Online Library on [31/01/2023]. See the Terms and Conditions (https://onlinelibrary.wiley.com/terms-and-conditions) on Wiley Online Library for rules of use; OA articles are governed by the applicable Creative Commons License